Modeling of Multiple Cycles for Sorption-Enhanced Steam Methane Reforming and Sorbent Regeneration in Fixed Bed Reactor

ARTICLE *in* ENERGY & FUELS · JULY 2007

Impact Factor: 2.79 · DOI: 10.1021/ef070112c

2 AUTHORS, INCLUDING:

Ningsheng Cai
Tsinghua University
136 PUBLICATIONS **1,790** CITATIONS

SEE PROFILE

Modeling of Multiple Cycles for Sorption-Enhanced Steam Methane Reforming and Sorbent Regeneration in Fixed Bed Reactor

Zhen-shan Li and Ning-sheng Cai*

Key Lab for Thermal Science and Power Engineering of MOE, Tsinghua University, Beijing 100084, China

Received March 5, 2007. Revised Manuscript Received June 7, 2007

Mathematical models of multiple cycles for sorption-enhanced steam methane reforming and Ca-based sorbent regeneration in a fixed bed reactor are developed. Empirical correlations are used to describe steam methane reforming, the water−gas shift, and CO_2 capture kinetics. The processes of multiple carbonation/calcination cycles of a Ca-based sorbent are taken into account to describe the sorption-enhanced hydrogen production process with the simultaneous removal of carbon dioxide by a Ca-based sorbent. The mathematical models are validated through comparing simulated results with experimental data. The model results qualitatively agree with experimental data. The effect of reactivity decay of dolomite, $CaO/Ca_{12}Al_{14}O_{33}$, and limestone sorbents on sorption-enhanced hydrogen production and sorbent regeneration processes was studied through numerical simulation. The simulated results indicated that the operation time of producing high-purity hydrogen (that is defined as the time for the start of breakthrough, often referred to as prebreakthrough time) declines continuously with the increasing of cyclic number due to the sorbent activity loss; the ultimate prebreakthrough time will remain nearly constant, due to the sorbent already reaching the final residual capture capacity. The ultimate prebreakthrough time is different for different sorbents. In comparison with dolomite and limestone sorbents, $CaO/Ca_{12}Al_{14}O_{33}$ sorbent can obtain a rather longer prebreakthrough time after a large cycle number due to its high reactivity and stability. After the reforming and CO_2 removal step, the Ca-based sorbents need to be regenerated to be used for the subsequent reforming cycle, and the multiple calcination processes of Ca-based sorbents under different calcination conditions are discussed.

1. Introduction

Hydrogen is considered to be a clean and important energy carrier for sustainable energy consumption. It can be widely used in the power and chemical industries, and it especially could be used as fuel in most appropriate fuel cells for minimal pollutant emissions and greenhouse gases. Hydrogen production from hydrocarbons mainly includes steam methane reforming (SMR), partial oxidation, autothermal reforming, and carbon dioxide reforming. Currently, on a commercial basis, the catalytic steam reforming of natural gas is the most economical process for producing hydrogen because it has the highest thermal efficiency and lowest capital investment. Although the SMR process has been used commercially for many years, there are still numerous limitations, Heat transfer nonuniformity, carbon deposition, and catalyst deactivation result in a much higher cost and lower efficiency.[1−3]

An approach to improve the conventional SMR process is to add a CO_2 acceptor into the reformer, which is also called a sorption-enhanced reforming process (SERP). According to Le Chatelier's principle, if CO_2 is removed as soon as it is formed, the reforming and water−gas shift (WGS) reactions proceed beyond the conventional thermodynamic limits and more methane would be converted to hydrogen. The SERP for the H_2 production has the following potential advantages over the conventional reforming process: high purity (95+%) hydrogen production in a single step, simplification of the hydrogen production process, no supplemental energy for the primary reactor and reduction of the heat exchangers, reduction of primary reactor operating temperature and pressure, and the reduction of the reactor material.

The important reactions in sorption-enhanced hydrogen production are as follows.

steam methane reforming (SMR):

$$CH_4 + H_2O = CO + 3H_2 \qquad \Delta H_{298} = 206.2\ \text{kJ/mol} \qquad \text{(I)}$$

water−gas shift (WGS):

$$CH_4 + 2H_2O = CO_2 + 4H_2 \qquad \Delta H_{298} = 164.7\ \text{kJ/mol} \qquad \text{(II)}$$

$$CO + H_2O = CO_2 + H_2 \qquad \Delta H_{298} = -41.5\ \text{kJ/mol} \qquad \text{(III)}$$

CO_2 sorption:

$$CO_2 + CaO = CaCO_3 \qquad \Delta H_{298} = -178\ \text{kJ/mol} \qquad \text{(IV)}$$

After the sorption-enhanced hydrogen production, CaO must be regenerated in a regenerator.

sorbent regeneration:

$$CaCO_3 = CaO + CO_2 \qquad \Delta H_{298} = 178\text{kJ/mol} \qquad \text{(V)}$$

Many research works about SERP and process development have been published, including the simultaneous reaction concept[4−5] and reaction equilibrium,[6] the shift reaction and carbon dioxide separation with calcium oxide in one reactor,[7] high-purity hydrogen production in a single reactor,[8] the

(1) Armor, J. N. *Appl. Catal. A, Gen.* **1999**, *176*, 159−176.
(2) Waldron, W. E.; Hufton, J. R.; Sircar, S. *AIChE J.* **2001**, *47*, 1477−1479.
(3) Harrison, D. P.; Peng, Z. Y. *Int. J. Chem. React. Eng.* **2003**, *1*, A37.

10.1021/ef070112c CCC: $37.00
Published on Web 07/14/2007

durability of dolomite in multicycle SERP tests,[9] a new hydrogen production by reaction-integrated novel gasification,[10] a zero-emission fuel cell vehicle system using SERP,[11] the sorption-enhanced H_2 production reactions at low pressures,[12] SERP using an atmospheric-pressure bubbling fluidized bed reactor,[13] and the effect of $Ca(OH)_2$ formation on SERP,[14] as well as continuous production of hydrogen from sorption-enhanced steam methane reforming in two parallel fixed bed reactors operated in a cyclic manner.[15]

In the literature, some researchers reported their modeling works on the SERP process. The model of SERP using K_2CO_3-promoted hydrotalcite as a CO_2 chemisorbent has been studied widely. On the basis of the adsorption equilibrium[16−17] and adsorption kinetics[17−18] of hydrotalcite-based high-temperature CO_2 adsorbents, dynamic reactor mathematical models for an adsorptive reactor were proposed and developed by Ding and Alpay[19] and the group led by Rodrigues.[20−23] However, only a few studies considered the dynamic behavior of steam methane reforming coupled simultaneous carbon dioxide removal by carbonation of a Ca-based sorbent for hydrogen production. Lee et al.[24] developed a dynamic model to describe the CaO carbonation-enhanced SMR reaction by assuming that the rate of the CaO carbonation in a local zone of the packed bed is limited by kinetics or by mass transfer limitation of the reactant CO_2. However, only a single sorption-enhanced reforming step was focused on. In practical application, the Ca-based sorbents are repeatedly used; that is, the sorbents must be regenerated in cycles after the carbonation reaction. Therefore, the repeated carbonation/calcination characteristics of sorbents are very important for SERP. The most common Ca-based absorbents suitable for the carbonation/calcination process, such as dolomite or limestone, undergo a decay of the CO_2 absorbed capacity.[25−26] The effect of reactivity decay of the Ca-based sorbent on the design and operation of a practical packed bed reactor should be studied.

The purposes of this study were as follows: (1) to develop the reactor model considering repeated carbonation/calcination cycles to analyze the SERP reactor system instead of studying a single-step reaction, and to validate the model using experimental data, (2) to study the variation of product gases' evolution profiles with reaction time for different sorbents using the developed model in order to discern the effects of the cycle number on sorption SERP, and (3) to study the effects of operational conditions on the calcination process and to determine the suitable operating conditions of a packed bed reactor.

2. Experimental Description

2.1. Carbonation and Calcination of Sorbent in Thermogravimetric Analyzer (TGA). A Dupont 951 TGA (TA Instrument 1200) machine was used to study the carbonation and calcination cycles of Ca-based CO_2 sorbents. Additional details can be found in the literature.[27] The following operating conditions were used for carbonation/calcination tests: (i) carbonation temperature, 923 K; calcination temperature, 1123 K; (ii) gas flow rate, 150 mL/min; (iii) gas compositions of CO_2/N_2, 5/95%, 8/92%, 15/85%, 20/80%, and 100/0%; (iv) solid amounts, 10∼15 mg. A three-way valve was used to switch between the pure nitrogen stream and the reaction gas mixture at certain carbonation and calcination time intervals. The times for carbonation and calcination are 30 and 5 min, respectively. $CaO/Ca_{12}Al_{14}O_{33}$ (75/25 wt %)[27−28] was chosen as the sorbent on the basis of earlier studies.

2.2. Sorption-Enhanced Hydrogen Production and Sorbent Regeneration Cycles in a Fixed Bed Reactor. Sorption-enhanced hydrogen production and sorbent regeneration cycles were carried out in a fixed bed reactor. The flow rates of CH_4, H_2, and Ar from high-purity cylinders were controlled using mass flow controllers. Water was fed as a liquid using a high-pressure pump. The combined feed gases and water entered near the top of the reactor and were preheated as they flowed downward in the preheater section in which quartz sand was packed. The reforming catalyst was a standard Ni-based catalyst, NiO/Al_2O_3 (∼20 wt % NiO), and $CaO/Ca_{12}Al_{14}O_{33}$ (75/25 wt %) was chosen as the sorbent on the basis of earlier studies. Before the reactions were carried out, the catalyst in the reactor was reduced in a flow of a H_2/Ar mixture (50 mol % hydrogen) at 873 K for 2 h. Both the catalyst and sorbent were crushed into powders with particle sizes in the range of 200−450 μm. Then, the preheated gas flowed downward through the mixture of reforming catalyst and CO_2 sorbent and exited at the bottom of the reactor. Excess steam was removed in the condenser. The product gases were analyzed using an AutoSystem XL gas chromatograph equipped with a thermal conductivity detector. The concentration of each component was the normalized concentration in volume percent assuming the total amounts of CH_4, H_2, CO, and CO_2 to be 100% after the removal of water by condensation. The progress of the regeneration reaction was followed by monitoring the CO_2 content in the product gases. Complete regeneration was achieved in all cycles for all tests.

3. Mathematical Model Description

3.1. The Model for Repeated Carbonation Reaction of Ca-Based Sorbents. The carbonation conversions of the CaO sorbent with time at temperatures 873−973 K and different CO_2

(4) Williams, R. Hydrogen Production. U.S. Patent 1,938,202, 1933.
(5) Gorin, E.; Retallick, W. B. Method for the Production of Hydrogen. U.S. Patent 3,108,857, 1963.
(6) Brun-Tsekhovoi, A. R.; Zadorin, A. N.; Katsobashvili, Y. R.; Kourdyumov, S. S. The Process of Catalytic Steam-Reforming of Hydrocarbons in the Presence of a Carbon Dioxide Acceptor. In *Hydrogen Energy Progress VII, Proceedings of the 7th World Hydrogen Energy Conference*, Moscow, Russia, Sept 25−29, 1988; Veziroglu, T. N., Protsenko, A. N., Eds.; Pergamon Press: New York, 1988; Vol. 2, p 885.
(7) Han, C.; Harrison, D. P. *Chem. Eng. Sci.* **1994**, *49*, 5875−5883.
(8) Balasubramanian, B.; Lopez, A.; Kaytakoglu, S.; Harrison, D. P. *Chem. Eng. Sci.* **1999**, *54*, 3543−3552.
(9) Ortiz, A. L.; Harrison, D. P. *Ind. Eng. Chem. Res.* **2001**, *40*, 5102−5109.
(10) Lin, S-Y; Suzuki, Y.; Hatano, H.; Harada, M. *Energy Convers. Manage.* **2002**, *43*, 1283−1290.
(11) Kato, Y.; Ando, K.; Yoshizawa, Y. J. *Chem. Eng. Jpn.* **2003**, *36*, 860−866.
(12) Yi, K. B.; Harrison, D. P. *Ind. Eng. Chem. Res.* **2005**, *44*, 1665−1669.
(13) Johnsen, K; Ryu, H. J.; Grace, J. R.; Lim C. J. *Chem. Eng. Sci.* **2006**, *61*, 1195−1202.
(14) Hildenbrand, N; Readman, J; Dahl, I. M.; Blom, R. *Appl. Catal., A* **2006**, *303*, 131−137.
(15) Li, Z. S.; Cai, N. S.; Yang, J. B. *Ind. Eng. Chem. Res.* **2006**, *45*, 8788−8793.
(16) Hufton, J. R.; Mayorga, S.; Sircar, S. *AIChE J.* **1999**, *45*, 248−256.
(17) Ding, Y; Alpay, E. *Chem. Eng. Sci.* **2000**, *55*, 3461−3474.
(18) Soares, J. L.; Moreira, R; José, H. J.; Grande, C.; Rodrigues, A. E. *Sep. Sci. Technol.* **2004**, *39*, 1989−2010.
(19) Ding, Y; Alpay, E. *Chem. Eng. Sci.* **2000**, *55*, 3929−3940.
(20) Xiu, G. H.; Soares, J. L.; Li, P.; Rodrigues, A. E. *AIChE J.* **2002**, *48*, 2817−2832.
(21) Xiu, G. H.; Li, P.; Rodrigues, A. E. *Chem. Eng. Sci.* **2003**, *58*, 3425−3437.
(22) Xiu, G. H; Li, P.; Rodrigues, A. E. *Chem. Eng. J.* **2003**, *95*, 83−93.
(23) Wang, Y. N.; Rodrigues, A. E. *Fuel* **2005**, *84*, 1778−1789.
(24) Lee, D. K.; Baek, I. H.; Yoon, W. L. *Chem. Eng. Sci.* **2004**, *59*, 931−942.
(25) Barker, R. *J. Appl. Chem. Biotechnol*. **1973**, *23*, 733−742.
(26) Abanades, J. C. *Chem. Eng. J.* **2002**, *90*, 303−306.
(27) Li, Z. S.; Cai, N. S.; Huang, Y. Y.; Han, H. J. *Energy Fuels* **2005**, *19*, 1447−1452.
(28) Li, Z. S.; Cai, N. S.; Huang, Y. Y. *Ind. Eng. Chem. Res.* **2006**, *45*, 1911−1917.

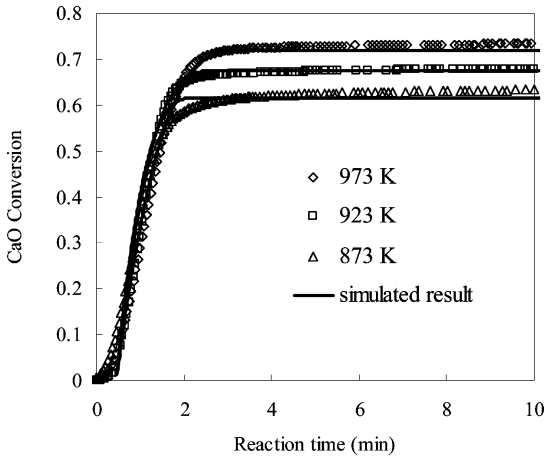

Figure 1. Conversion of $CaO/Ca_{12}Al_{14}O_{33}$ (75/25 wt %) when carbonated at 873−973 K (15% CO_2, 85% N_2) in TGA.

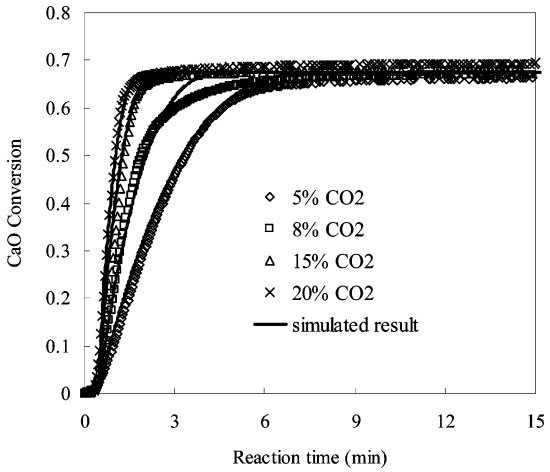

Figure 2. Conversion of $CaO/Ca_{12}Al_{14}O_{33}$ (75/25 wt %) under 5−20 vol % CO_2 carbonated at 923 K in TGA.

fractions in the atmosphere are shown in Figures 1 and 2. It can be seen from Figure 1 that the carbonation rate is independent of temperature in the range of 873−973 K; this result is consistent with the early studies finished by Bhatia and Perlmutter,[29] and the ultimate conversion of CaO is independent of the CO_2 fraction but increases with an increase in the reaction temperature. Our experimental results also show that the CO_2 fraction has some effect on the carbonation rate, as shown in Figure 2; the carbonation rate becomes more rapid when the CO_2 fraction increases. The effect of total pressure on the carbonation reaction is complex. The CO_2 concentration increases proportionally with an increase in the total pressure, and the bulk diffusion coefficient varies inversely with the pressure so that the effect of increased concentrations tends to be neutralized. If Knudsen diffusion in small pore dimensions is rate-controlling, the diffusion coefficient is independent of the pressure; however, the mass flux increases with the total pressure. The increase in CO_2 concentration with the total pressure would not appreciably increase the rate of carbonation,[30] and Sun et al. also observed that changes in the total pressure had little influence on CO_2 removal in the carbonation process.[31] Therefore, it is assumed that CaO carbonation can be expressed as the following semiempirical equation:

$$\frac{dX}{dt} = k_c\left(1 - \frac{X}{X_u}\right)^{2/3}(C_{CO_2} - C_{e.CO_2})^{(P/P_0)^{0.083}} \quad (1)$$

Except for the correcting term $(P/P_0)^{0.083}$ to account for the effect of total atmospheric pressure on the carbonation rate, eq 1 is similar to early studies reviewed by Bhatia and Perlmutter.[29] With the experimental result as shown in Figures 1 and 2, the values of k_c and X_u can be obtained and are as follows:

$$k_c = 8.124 \quad (2)$$

The apparent kinetic expression for CaO carbonation was used

$$X_u = 0.1097(T/100) - 0.3391 \quad (873\ \text{K} < T < 973\ \text{K}) \quad (3)$$

for multicycles of carbonation/calcination:

$$\frac{dX_N}{dt} = k_c\left(1 - \frac{X_N}{X_{u,N}}\right)^{2/3}(C_{CO_2} - C_{e.CO_2})^{(P/P_0)^{0.083}} \quad (4)$$

where X_N and $X_{u,N}$ denote the fractional conversion of CaO to $CaCO_3$ and the ultimate conversion of CaO in the Nth cycle, respectively.

The molar rate of CO_2 removal per kilogram of CaO, $R_{cbn,N}$, in the Nth cycle can be represented as a function of the fractional conversion of CaO, X_N:

$$R_{cbn,N} = \frac{\eta_{sorbent}}{M_{CaO}}\frac{dX_N}{dt} \quad (5)$$

Equation 4, which is also identical to the one obtained with the spherical grain model of Szekeley et al.,[32] is used to calculated the conversion rate of a single CaO particle in TGA. However, all sorbent and catalyst particles are mixed and packed together in fixed bed reactor, and the mass transfer of CO_2 toward the particle of sorbent and intraparticle diffusion in the fixed bed reactor both have some effect on the carbonation rate. At the same time, other gas components (H_2, CH_4, CO, and H_2O) may also have some effect on the conversion rate of CaO. A detailed description of these phenomena is beyond the scope of this paper; to simplify things, a parameter, $\eta_{sorbent}$, is introduced in eq 5 to take into account these factors.

The CaO carbonation conversion increase in a time increment Δt can be calculated as

$$X_{N,t+\Delta t} = X_{N,t} + M_{CaO}\int_t^{t+\Delta t} R_{cbn,N}\,dt \quad (6)$$

3.2. The Model for Repeated Calcination Reaction of Ca-Based Sorbents. Figure 3 shows the evolution of $CaCO_3$ conversion with calcination time with different CO_2 fractions in a calcination atmosphere for the $CaO/Ca_{12}Al_{14}O_{33}$ (75:25 wt %) sorbent. The carbonation was carried out at 923 K and 20% CO_2 for 30 min; then, the sample was calcined with the temperature of TGA beginning to increase from 923 to 1123 K.

(29) Bhatia, S. K.; Perlmutter, D. D. *AIChE J.* **1983**, *29*, 79−86.
(30) Kyaw, K.; Kanamori, M.; Matsuda, H.; Hansatani, M. *J. Chem. Eng. Jpn.* **1996**, *29*, 112−118.
(31) Sun, P.; Grace, J. R.; Lim, C. J.; Anthony, E. J. *Energy Fuels* **2007**, *21*, 163−170.
(32) Szekeley, J.; Evans, J. W.; Sohn, H. Y. *Gas-Solid Reactions*; Academic Press: London, 1976.

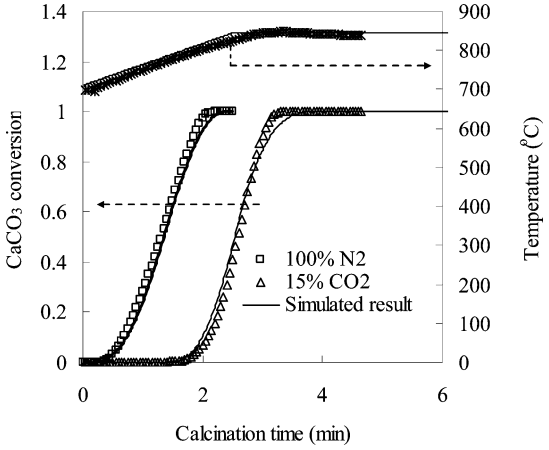

Figure 3. Conversion of $CaCO_3$ to CaO with time in TGA (the temperature-raising rate of TGA was 54 °C/min).

The apparent kinetic model for the conversion rate of $CaCO_3$ to CaO can be expressed as

$$\frac{dX_{calci}}{dt} = k_{calci}(1 - X_{calci})^{2/3}\left(1 - \frac{P_{0,CO_2}}{P_{e,CO_2}}\right)^{1.86} \quad (7)$$

here P_{e,CO_2} is the partial equilibrium pressure of CO_2:[33]

$$P_{e,CO_2} = 1.826 \times 10^{12} \exp\left(-\frac{19\,680}{T}\right) \quad (8)$$

P_{0,CO_2} is the fractional partial pressure of CO_2 in gas phase, Pa.

The chemical reaction rate constant for the $CaCO_3$ calcination process is

$$k_{calci} = 5.61 \times 10^5 \exp\left(-\frac{150\,000}{RT}\right) \quad (9)$$

The simulated results of $CaCO_3$ calcination are also shown in Figure 3. It can be seen that the CO_2 fraction has an important effect on the $CaCO_3$ calcination process. At the same rate of increasing temperature, the decomposition temperature of $CaCO_3$ increases with the increase in the CO_2 fraction. From eq 7, $CaCO_3$ decomposition has been affected by the CO_2 partial pressure P_{0,CO_2} and CO_2 equilibrium pressure P_{e,CO_2}. P_{e,CO_2} increases with the increasing of temperature, and the difference between P_{e,CO_2} and P_{0,CO_2} will also increase, resulting in an accelerated CO_2 decomposition rate. The increasing of the CO_2 fraction increases the value of P_{0,CO_2}, while it reduces the difference between P_{e,CO_2} and P_{0,CO_2}, resulting in a high initial decomposition temperature at the same rate of increasing temperature. When the calcination temperature is low, P_{e,CO_2} is smaller than P_{0,CO_2}, and the decomposition reaction of $CaCO_3$ will not happen. Only when the calcination temperature approaches the value at which the difference between P_{e,CO_2} and P_{0,CO_2} is larger than zero can the decom- position reaction happen, as shown in Figure 3. It also can be seen from the comparison of simulated results with experimental results, as shown in Figure 3, that the mathematical model can predict good results for the $CaCO_3$ calcination process.

The molar rate of CO_2 production per kilogram of $CaCO_3$, R_{calci}, in the calcination process can be represented as a function of the fractional conversion rate of $CaCO_3$:

$$R_{calci} = \frac{\eta_{sorbent}}{M_{CaCO_3}} \frac{dX_{calci}}{dt} \quad (10)$$

The $CaCO_3$ calcination conversion increase at a time increment Δt can be calculated as

$$X_{calci,t+\Delta t} = X_{calci,t} + M_{CaCO_3} \int_t^{t+\Delta t} R_{calci}\, dt \quad (11)$$

3.3. Reforming and Shift Reaction Kinetics. Xu and Froment[34] gave the reaction kinetic model of reforming and shift reations:

$$R_I = \frac{1}{(DEN)^2} \frac{k_1}{P_{H_2}^{2.5}} \left(P_{CH_4} P_{H_2O} - \frac{P_{H_2}^3 P_{CO}}{K_I}\right) \quad (12)$$

where P_i is the gas-phase pressure fraction of component i.

$$R_{II} = \frac{1}{(DEN)^2} \frac{k_2}{P_{H_2}^{3.5}} \left(P_{CH_4} P_{H_2O}^2 - \frac{P_{H_2}^4 P_{CO_2}}{K_{II}}\right) \quad (13)$$

$$R_{III} = \frac{1}{(DEN)^2} \frac{k_3}{P_{H_2}} \left(P_{CO} P_{H_2O} - \frac{P_{H_2} P_{CO_2}}{K_{III}}\right) \quad (14)$$

$$DEN = (1 + K_{CO}P_{CO} + K_{H_2}P_{H_2} + K_{CH_4}P_{CH_4} + K_{H_2O}P_{H_2O}/P_{H_2}) \quad (15)$$

3.4. Governing Equations. For component i, the mass balance for the fixed-bed reactor in the SERP step can be written as

$$\epsilon_b \frac{\partial C_i}{\partial t} + \frac{\partial (uC_i)}{\partial z} - (1 - \epsilon_b)\rho_{b,cat} \sum_{j=I}^{III} \upsilon_{ij}\eta_j R_j - (1 - \epsilon_b)\rho_{b,CaO} R_{cbn,N} = 0 \quad (i = H_2, CO, CO_2, CH_4, H_2O) \quad (16)$$

The mass balance for the calcination step can be written as

$$\epsilon_b \frac{\partial C_i}{\partial t} + \frac{\partial (uC_i)}{\partial z} - (1 - \epsilon_b)\rho_{b,CaCO_3,N} R_{calci} = 0 \quad (i = CO_2) \quad (17)$$

where C_i is the molar concentration of species i, ϵ_b is the bed void fraction, u is the superficial velocity, $\rho_{b,cat}$ is the density of the catalyst of the bed, $\rho_{b,CaO}$ is the density of the CaO of the bed and can be written as $\rho_{b,CaO} = (W_{sor}X_{active})/(1 - \epsilon_b)$, and $\rho_{b,CaCO_3,N}$ is the density of the $CaCO_3$ of the bed in N cycles and can be written as

$$\rho_{b,CaCO_3,N} = \frac{W_{CaCO_3,N}}{1 - \epsilon_b} = \frac{W_{sor}X_{active}X_{u,N}}{1 - \epsilon_b} \frac{M_{CaCO_3}}{M_{CaO}} \quad (18)$$

The energy balance for the fixed bed in the SERP step can be written as

(33) Hu, N. Y.; Scaroni, A. W. *Fuel* **1996**, *75*, 177−186.

(34) Xu, J.; Froment, G. F. *AIChE J.* **1989**, *35*, 88−96.

$$[(1-\epsilon_b)\rho_s C_{ps} + \epsilon_b \rho_g C_{pg}]\frac{\partial T}{\partial t} + \rho_g C_{pg} u \frac{\partial T}{\partial z} + (1-\epsilon_b)\,\rho_{b,CaO} R_{cbn,N} \Delta H_{carbo,CO_2} + (1-\epsilon_b)\rho_{b,cat} \sum_{j=I}^{III} \eta_j R_j \Delta H_{R,j} - \frac{2U}{R_0}(T_W - T) = 0 \quad (19)$$

The energy balance for the calcination step can be written as

$$[(1-\epsilon_b)\rho_s C_{ps} + \epsilon_b \rho_g C_{pg}]\frac{\partial T}{\partial t} + \rho_g C_{pg} u \frac{\partial T}{\partial z} + (1-\epsilon_b)\,\rho_{b,CaCO_3,N} R_{calci} \Delta H_{calci,CO_2} - \frac{2U}{R_0}(T_W - T) = 0 \quad (20)$$

The average apparent density of the catalyst and sorbent in the reactor, ρ_s, can be written as $\rho_s = \rho_{b,cat} + \rho_{b,sor}$; W_{cat} and W_{sor} are the weights of the catalyst and Ca-based sorbent in the fixed bed reactor, respectively. C_{ps} and C_{pg} are the gas and solid phase heat capacity, respectively; $\Delta H_{carbo,CO_2}$ is the reaction heat of carbonation; $\Delta H_{R,j}$ is the reaction heat of j (j = I, II, and III); U is the overall bed-wall heat-transfer coefficient,[22] and R_0 is the inner radius of the reactor.

3.5. Numerical Discretization and Model Solution. The initial conditions are as follows:

$$T = T_{init}, C_i = C_{i,init} \text{ at } t = 0 \; (i = H_2, CO, CO_2, H_2O, \text{and } CH_4) \quad (21)$$

The boundary conditions are as follows:

$$(C_i)_{z=0} = C_{i,f}, (u)_{z=0} = u_f, (P)_{Z=0} = P_H, (T)_{z=0} = T_f, \text{ at } z = 0 \quad (22)$$

Equations 16, 17, 19, and 20 were discretized to a set of ordinary differential equations with initial conditions. The reactor was divided into 50 sections with 51 nodes along the axis direction. The "ode15s.m" stiff-variable integrated in the time domain method in MATLAB was used to obtain the effluent mole fraction and temperature distribution along the reactor.

4. Results and Discussion

4.1. Model Verification and Analysis. The simulation results of SERP and the sorbent calcination cycle were validated by the experimental data from the fixed bed reactor, as shown in Figures 4 and 6. A summary of the values of the parameters used in the simulation is given in Table 1. The experimental and simulated results of SERP are shown in Figure 4 where the mole percentages (dry basis) of H_2 in the product gas are plotted versus time. It can be seen from Figure 4 that the simulation results agreed with experimental data well for the SERP step. Figure 4 is divided into three regions indicated by the vertical dotted lines. In the prebreakthrough period, the hydrogen concentration is higher than 90 vol % on a dry basis for a period of 45 min. During the prebreakthrough period, the reforming, shift, and CO_2 separation reactions occur at maximum efficiency, and the mole percent of each component in the product gas is very near the respective equilibrium values.[9] In the breakthrough period, the CO_2 removal efficiency of the sorbent begins to decrease, which reduces the extents of the reforming and shift reactions, resulting in a decrease in the H_2 content. When the sorbent approaches its maximum conversion, the CO_2 separation reaction is no longer effective and the postbreakthrough period begins. Only the reforming and shift reactions happen in this period.

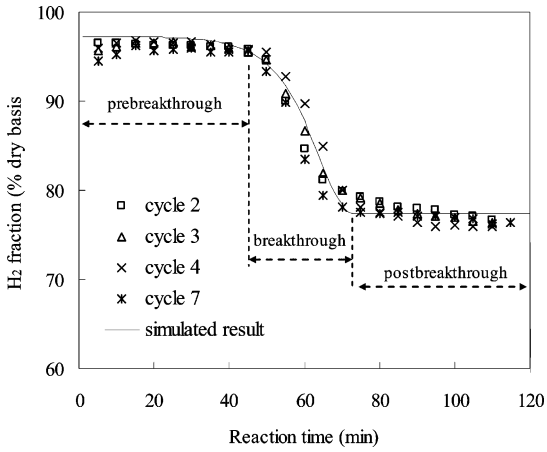

Figure 4. H_2 fraction on a dry basis during SERP step for different cycles; comparison of the simulation with the experiment in the fixed bed reactor (temperature = 923 K, pressure = 1 atm, feed CH_4 = 20 mL/min, H_2O/CH_4 = 4, $CaO/Ca_{12}Al_{14}O_{33}$ as sorbent).

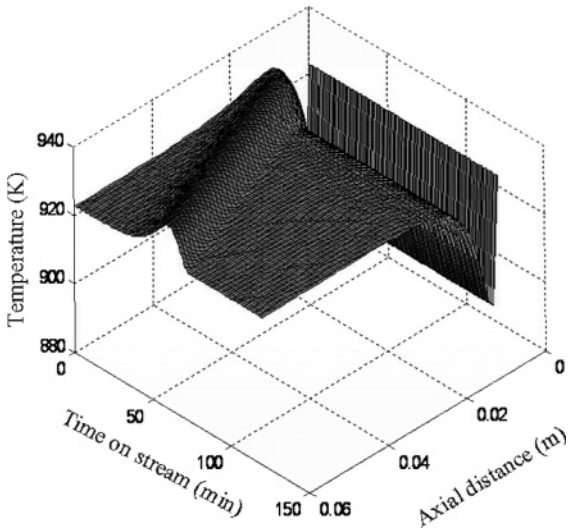

Figure 5. Time-dependent spatial distribution of fixed bed reactor temperature in SERP period.

Table 1. Values of Parameters Used in Simulation

parameter	value	parameter	value
C_{pg}	8.45 kJ/(kg K)	W_{sor}	4.67×10^{-3} kg
C_{ps}	0.98 kJ/(kg K)	W_{cat}	3.33×10^{-3} kg
d_p	3×10^{-4} m	ϵ_b	0.5
R_0	0.9×10^{-2} m	η_I, η_{II}, η_{III}	0.3
L	6×10^{-2} m	P	1 atm
T	923 K	H_2O/CH_4	4
η_{CaO}	0.2	CH_4	20 mL/min
		Ar	180 mL/min (calcination step)

The reaction-time-dependent axial distributions of the fixed bed temperature are shown in Figure 5. The temperature near the reactor bed entrance rapidly drops to about 890 K from the initial 923 K; this is because the endothermic reforming reaction in this region is faster than the exothermic CaO carbonation reaction, resulting in a large temperature decrease. The temperature drop lasts a long period of time. In the subsequent bed location after this cool bed region, the carbonation reaction of CaO in the fixed bed is dominant; the exothermic heat of the carbonation reaction is used to heat up this region, and therefore, the local temperature of a bed region increases as shown in Figure 5. A maximum increase in the temperature to 15 K above

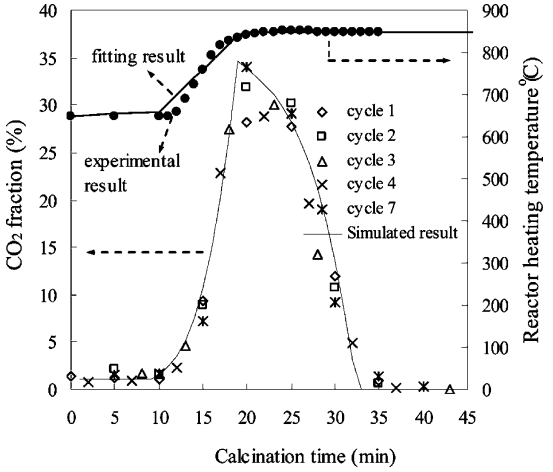

Figure 6. CO_2 fraction during sorbent calcination step; comparison of the simulation with the experiment in fixed bed reactor (pressure = 1 atm, feed Ar = 180 mL/min, $CaO/Ca_{12}Al_{14}O_{33}$ as sorbent).

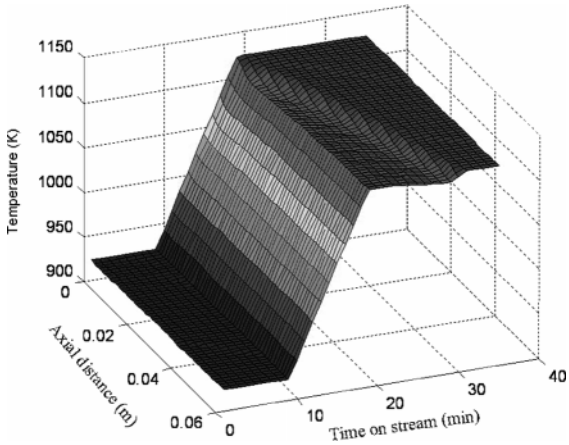

Figure 7. Time-dependent spatial distribution of fixed bed reactor temperature in calcination period (pressure = 1 atm, feed Ar = 180 mL/min, $CaO/Ca_{12}Al_{14}O_{33}$ as sorbent).

the initial temperature can be observed, and the bed zone with such a temperature increase moves toward the reactor exit with the reaction time on stream.

The postbreakthrough period was stable for a period of 40∼60 min for each cycle; then the flows of CH_4 and H_2O were stopped, and the flow of Ar was introduced into the reactor. When the CO_2 concentration from gas chromatograph (GC) approached a small value, the temperature of the reactor was adjusted to 1123 K and kept stable for some time to completely recalcinate $CaCO_3$ and reactivate the sorbent. When the CO_2 concentration from GC approached a small value again, the process of $CaCO_3$ decomposition was considered to be finished, and the temperature of the reactor was reduced to 923 K again and kept stable for some time. Then, the flow rate of Ar was stopped, and CH_4 and H_2O were fed into the reactor again. The decomposition rate of $CaCO_3$ in an Ar atmosphere at 923 K is very little, as shown in Figure 6; therefore, the progress of $CaCO_3$ decomposition at 923 K is considered to have no effect on the amount of CO_2 released during the regeneration period. Figure 6 showed the CO_2 fraction during the regeneration period as a function of time for 1∼4 and 7 cycles. The reactor temperature was gradually raised to 1123 K from 923 K during the regeneration period, the decomposition rate of $CaCO_3$ was also accelerated with the increasing of the reactor temperature, resulting in the CO_2 fraction increasing gradually with time, as shown in Figure 6. When the reactor temperature approached 1123 K, the decomposition rate of $CaCO_3$ was accelerated largely, and the CO_2 fraction approached the maximum. With the increasing of regeneration time, the fraction of $CaCO_3$ uncalcined in the reactor decreased and the CO_2 fraction began to decrease with time. When all of the $CaCO_3$ was calcined, no CO_2 was released, and the CO_2 concentration approached zero at this time. It can be seen from Figure 6 that the simulation results agreed with experimental data well for the calcination step.

The reaction-time-dependent axial distributions of the fixed bed temperature in the calcination period are shown in Figure 7. After the postbreakthrough period, the flows of CH_4 and H_2O were stopped and the flow of Ar was introduced into reactor. When the CO_2 concentration from the GC approached a small value, the temperature of the reactor was increased gradually to 1123 K from 923 K. It can be seen from Figure 7 that there was a region where the reactor temperature dropped; this is because the endothermic calcination reaction in this region happens, resulting in the temperature decrease. The temperature drop lasts a long period of time, and the bed zone with such a temperature decrease moves toward the reactor exit with the reaction time on stream.

4.2. Effect of Sorbent Multiple Carbonation/Calcinatino Cycles on the SERP Process. Many researchers found that the conversion of CaO to $CaCO_3$ in the carbonation step decreases with an increase in the cyclic number of carbonation/calcination. On the basis of published experimental data on repeated carbonation/calcination cycles of CaO for a great range of different conditions, Abanades and Alvarez[35] developed a formula and discussed CaO reactivity decay characteristics. The decay behavior of the sorption capacity has been examined, and Wang and Anthony[36] have proposed a new simple equation. Recently, Abanades and Grasa[37] tested long series of carbonation/calcination cycles (up to 500 cycles) varying different variables that affect sorbent capacity and found a residual conversion of about 7−8% that remains constant after many hundreds of cycles and that seems insensitive to process conditions. A semiempirical equation (eq 23) has been proposed by Abanades and Grasa[37] to describe sorbent conversion loss with the number of cycles based on these new long data series.

$$X_{u,N} = \frac{1}{\dfrac{1}{1 - X_r} + kN} + X_r \qquad (23)$$

X_r is the residual conversion of the Ca-based sorbent after many cycles, and k is the deactivation constant. In this work, eq 23 which described the activity decay of Ca-based CO_2 sorbents was used to describe the reactivity loss of three Ca-based sorbents for many cycles of carbonation/calcination, and the value of k was different for different sorbents and was determined from experimental result fitting.

The regeneration temperature for $CaCO_3$ decomposition in the SERP system is critical and governed by the thermodynamics of the regeneration system. A temperature range from 1073 K without a CO_2 stream in the calcination atmosphere at 1 atm to 1173 K with a 100% CO_2 stream at 1 atm is required. When the heat for sorbent regeneration is provided by the combustion of the fuel−air mixture inside the regenerator, such as unmixed reforming for the small-scale generation of hydrogen,[38] the

(35) Abanades, J. C.; Alvarez, D. *Energy Fuels* **2003**, *17*, 308−315.
(36) Wang, J.; Anthony, E. J. *Ind. Eng. Chem. Res.* **2005**, *44*, 627−629.
(37) Grasa, G. S.; Abanades, J. C. *Ind. Eng. Chem. Res.* **2006**, *45*, 8846−8851.
(38) Lyon, R. K.; Cole, J. *Combust. Flame*. **2000**, *121*, 249.

Table 2. The Value of k and X_r in eq 23

sorbent (calcination temperature)	k	X_r	ref
dolomite (1123 K)	0.04	0.23	9
dolomite (1273 K)	0.39	0.11	37
$CaO/Ca_{12}Al_{14}O_{33}$ (1253 K)	0.06	0.16	27−28
limestone (1223 K)	0.52	0.075	37

Table 3. Values of Parameters Used in Simulation for Dolomite, Limestone, and $CaO/Ca_{12}Al_{14}O_{33}$ Sorbents

parameter	value	parameter	value
particle size	200∼425 μm	sorbent mass	2.6×10^{-2} kg
temperature	650 °C	catalyst mass	1.4×10^{-2} kg
pressure	15 atm	H_2O/CH_4	4
reactor length	12.7×10^{-2} m	CH_4 flow rate	60 mL/min
reactor diameter	1.9×10^{-2} m	N_2 flow rate	200 mL/min

regeneration process of Ca-based sorbents can operate under mild calcination conditions. The values of k and X_r in eq 23 for a dolomite sorbent at 1123 K under mild calcination conditions are shown in Table 2. Eight different repeated carbonation/calcination cycle cases are considered in this simulation, with an aim to study the effect of the carbonation/calcination number on high-purity hydrogen production. The parameters used in this simulation are shown in Table 3. The evolution profiles of product gas fractions with the reaction time at different carbonation/calcination cycles using the developed model are shown in Figure 8. It should be noted that the feed gas in the experimental tests contained a significant amount of N_2 diluent. That is the reason that the maximum H_2 concentrations in the experiments and the model were limited to just greater than 50%. This is not an inherent limitation of the SERP process. Experimental results for cycles 2, 15, and 25 from Ortiz and Harrison[9] are also shown in Figure 8 to validate the model. As shown in Figure 8, except for some scattered experimental data for CO concentration, good agreement exists between the experiment and the simulation for the 2nd, 15th, and 25th cycles. In the second cyclic cycle of SERP, the time for the reaction enhancement in H_2 production is about 75 min with a lower concentration of CO, CO_2, and CH_4 in the product gas due to CO_2 in situ removal by the carbonation of CaO in the reactor bed. However, with an increase in the carbonation/calcination cycle, the prebreakthrough time decreases continuously due to the decay of CaO activity. The decline of CO_2 sorption capacity with the increasing carbonation/calcination cycles can be attributed to the particle textural changes during calcination. After the reaction of CaO with CO_2, the reaction product $CaCO_3$ must undergo the calcination process in order to regenerate CaO to be used repeatedly. In the process of calcination, some pores are produced inside the CaO particle; at the same time, CaO sintering happens during high-temperature calcination. When small CaO particles are heated to a certain temperature that is high enough yet below the melting point, CaO coalesces and sinters, and the surface of nascent CaO decreases with the increase in residence time. Surface and porosity are very important for the reaction of CaO with CO_2, but sintering reduces surface area and porosity sharply, which in turn affects the reaction rates of CaO with CO_2.[27,35] When the repeated carbonation/calcination cycle for dolomite is larger than 500, the prebreakthrough time almost does not decrease; this is because dolomite already approaches its lowest ultimate conversion (X_r) after 500 cycles. Finally, the lowest prebreakthrough time for dolomite sorbent calcined at 1123 K can last 10 min due to the existence of a residual conversion; this is very important in the design and operation of SERP systems using carbonation and calcination cycles.

If the processes of methane steam reforming with Ca-based sorbent addition are operated in pursuit of as large a CO_2 sequestration as possible and large production of hydrogen, the regeneration of the Ca-based CO_2 sorbent happens in a pure CO_2 stream and at higher calcination temperatures. Hence, the performance of the Ca-based sorbent needs to be evaluated at higher concentrations of CO_2 and higher calcination temperatures in every cycle during regeneration. The values of k and X_r in eq 23 are specific to the sorbents calcined at higher temperatures and are shown in Table 2. A comparison between experimental and modeling results is shown in Figure 9.

The cyclic reaction simulation results of SERP with $CaO/Ca_{12}Al_{14}O_{33}$, dolomite, and limestone as the sorbent are shown in Figures 10−12. In comparison with the dolomite sorbent, the prebreakthrough period of $CaO/Ca_{12}Al_{14}O_{33}$ can last a rather longer time at a large cyclic number due to its high reactivity and stability. Limestone is also regarded as a conventional CO_2 sorbent and has been tested by many researchers. Though it contains more CaO compared to dolomite and $CaO/Ca_{12}Al_{14}O_{33}$, it suffers a rapid decay of reactivity with the increase of the cyclic number. To illustrate the effects of different sorbents on the hydrogen production process, multiple SERP cycles with limestone as the sorbent are also simulated, and the calculated results are shown in Figure 12. The first sorption-enhanced SMR reaction with limestone as the CO_2 sorbent is similar to that of dolomite and $CaO/Ca_{12}Al_{14}O_{33}$, and the sorption-enhanced period lasts a long time. However, at the 15th cycle, the duration of the sorption-enhanced period decreases drastically. From the 500th cyclic number, the prebreakthrough time is constant due to the existence of a residual conversion; this is similar to the case of dolomite, as shown in Figures 11 and 12.

As a summary for some results above about the mutltiple cycles of SERP, it should be mentioned that the CaO sorbent can still give an enhancement to the SMR reaction after many carbonation/calcination cycles. Figure 13 shows the variation of prebreakthrough time with the cyclic number for different sorbents. It can be concluded that in cyclic SERP the feasible prebreakthrough time for the reaction and sorption step is mainly determined by the cyclic sorption capacity of the sorbent. It is shown in Figure 13 that, with the increase in sorbent cyclic capacity, the prebreakthrough time increases also. For three types of sorbents, with the increase in cyclic number, the prebreakthrough time declines continuously. With a further increase of the cycle, the prebreakthrough time will remain nearly constant, due to the sorbent already reaching the final residual capture capacity. When designing or operating the SERP system, if the prebreakthrough time is assumed to be no less than 15 min, the maximum cyclic numbers for limestone and dolomite are 50 and 15 cycles, respectively. If the cyclic number is larger than the maximum cyclic number, a makeup flow of the sorbent is required to compensate for the decay of activity loss during the subsequent cycle in order to obtain high-purity hydrogen in the 15 min prebreakthrough period. In this case, coupled fluidized bed reactors would be superior to fixed beds, because the makeup and purge could be more easily accomplished, and the result would be steady-state operation. But for the $CaO/Ca_{12}Al_{14}O_{33}$ sorbent, a makeup flow of the sorbent is not required, as shown in Figure 13. Because of different cyclic sorption capacities for different sorbents, the ultimate prebreakthrough time is also different. For limestone and dolomite sorbents, which suffer from a rapid decline of sorption capacity, the final prebreakthrough time is 11 and 6 min, respectively. Among the above sorbents, $CaO/Ca_{12}Al_{14}O_{33}$ obtains the highest

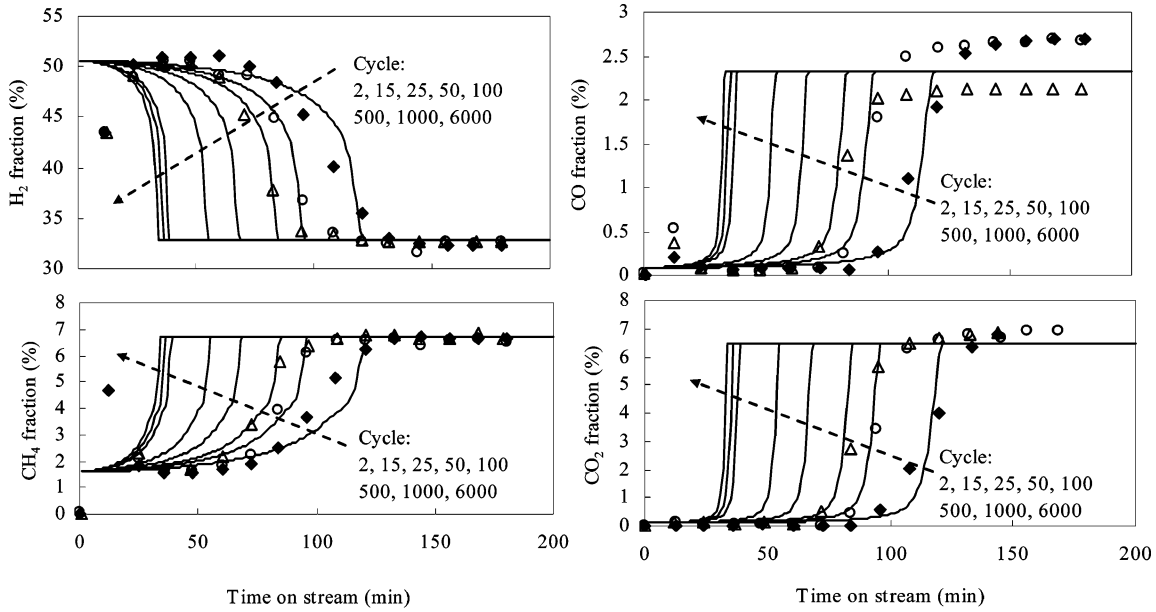

Figure 8. Product gas compositions in 6000-cycle simulation following in situ regeneration at 1123 K in N_2 for dolomite sorbent; comparison of the simulation with partial experiment in 25-cycle test (sorbent was dolomite and the experimental results were obtained from the literature[9]).

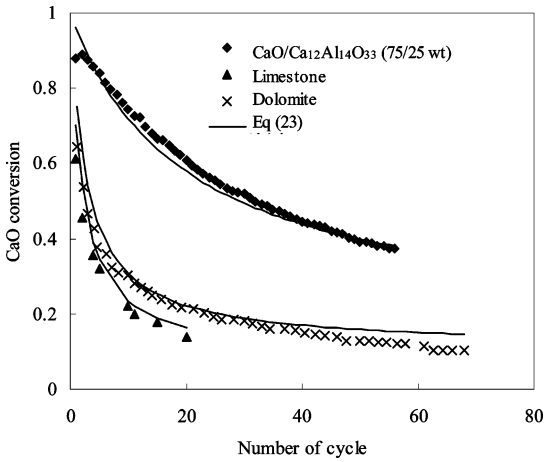

Figure 9. Comparison between experimental and modeling results of sorbent activity loss for three sorbents calcined at higher temperature.

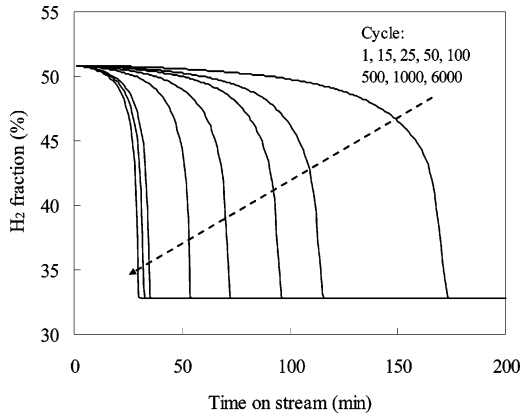

Figure 10. H_2 fraction in 6000-cycle simulation following in situ regeneration at higher temperature for $CaO/Ca_{12}Al_{14}O_{33}$ sorbent.

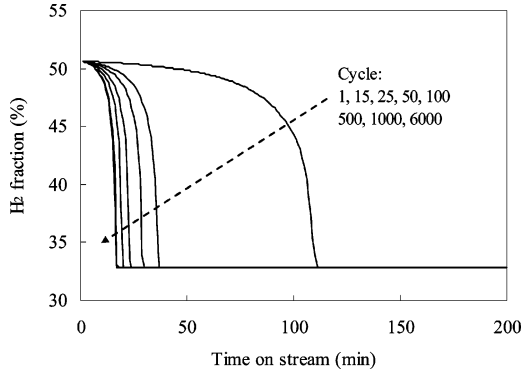

Figure 11. H_2 fraction in 6000-cycle simulation following in situ regeneration at higher temperature for dolomite sorbent.

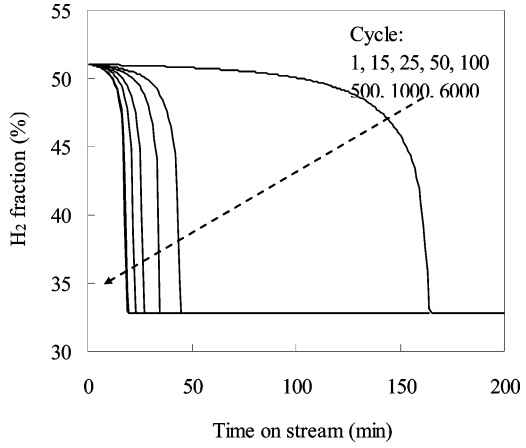

Figure 12. H_2 fraction in 6000-cycle simulation following in situ regeneration at higher temperature for limestone sorbent.

multicycle durabilities and the maximum residual capture capacity; the final prebreakthrough time is 15 min.

The costs of limestone and dolomite are $26.70/ton and $30/ton, respectively.[39] The cost of $CaO/C_{12}Al_{14}O_{33}$ (75/25 wt %) was $130/ton, which was determined assuming that limestone and Al_2O_3 ($500/ton) are the main components during fabrication, to which a 20% manufacturing cost was added. As they are naturally occurring materials, the cost of limestone and dolomite is quite low; it is obvious that a synthesized sorbent with high performance and a low cost would be highly beneficial for the sorption-enhanced hydrogen production process.

(39) *Mineral Commodities Suymmaries 2005*; U.S. Gelogical Survey, United States Government Printing Office: Washington, DC, 2005 (available at http://minerals.usgs.gov/minerals).

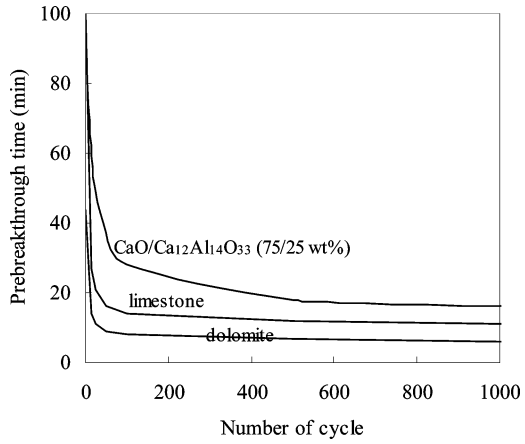

Figure 13. Variation of prebreakthrough time over cycle number for three sorbents calcined at higher temperature.

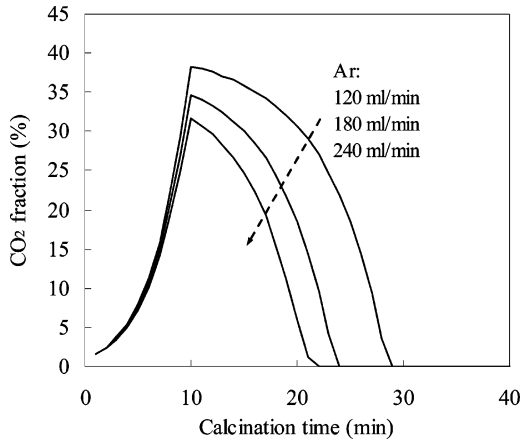

Figure 14. Evolution of CO_2 fraction with calcination time during sorbent regeneration period for different Ar flow rate (sorbent is CaO/$Ca_{12}Al_{14}O_{33}$ and calcination conditions are seen Table 1).

4.3. Effects of Operational Conditions and Sorbent Activity Decay on the Calcination Process. After the reforming and in situ CO_2 removal step, the Ca-based sorbents need to be regenerated to be used for the subsequent reforming cycle. Figure 14 shows the effect of the Ar flow rate on the CO_2 fraction during the sorbent regeneration period for the first cycle with the same rate of increasing temperature and calcination temperature (1123 K). It can be seen that the CO_2 fraction and the time for the complete decomposition of $CaCO_3$ decrease with the increase in Ar flow rate. This is because P_{0,CO_2} decreases with the increase in Ar flow rate, and the difference between P_{e,CO_2} and P_{0,CO_2} will increase, thus accelerating the CO_2 decomposition rate.

If carbon capture and sequestration is considered in the system of SERP, the regeneration of Ca-based CO_2 sorbents happens in a pure CO_2 stream or a mixture of CO_2 and H_2O at higher calcination temperatures. The regeneration temperature for $CaCO_3$ decomposition in the SERP system is governed by the thermodynamics of the regeneration system. From thermodynamic calculations, a CO_2 partial pressure of nearly 1 atm can be achieved for $CaCO_3$ decomposition for a temperature of 1173 K. However, to ensure the complete calcination of $CaCO_3$, the regenerator should be operated at a slightly higher temperature. In the stead of pure CO_2, steam can also be introduced into the fixed bed reactor as a purge gas in the sorbent step in order to decrease the calcination temperature. After steam is removed in the condenser, pure CO_2 can be obtained. Figure 15 shows the effect of different calcination temperatures on the sorbent

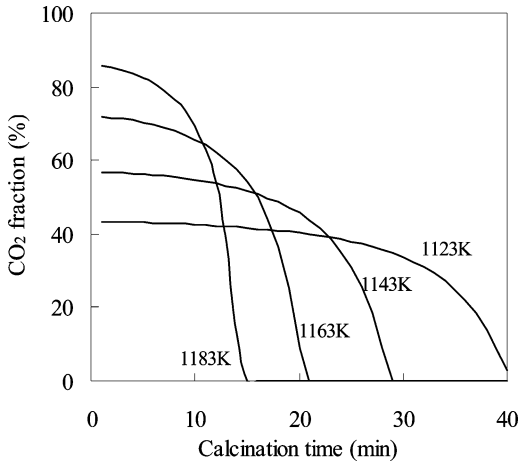

Figure 15. Evolution of CO_2 fraction with calcination time during sorbent regeneration period for different calcination temperature (sorbent is CaO/$Ca_{12}Al_{14}O_{33}$, steam flow rate = 50 mL/min).

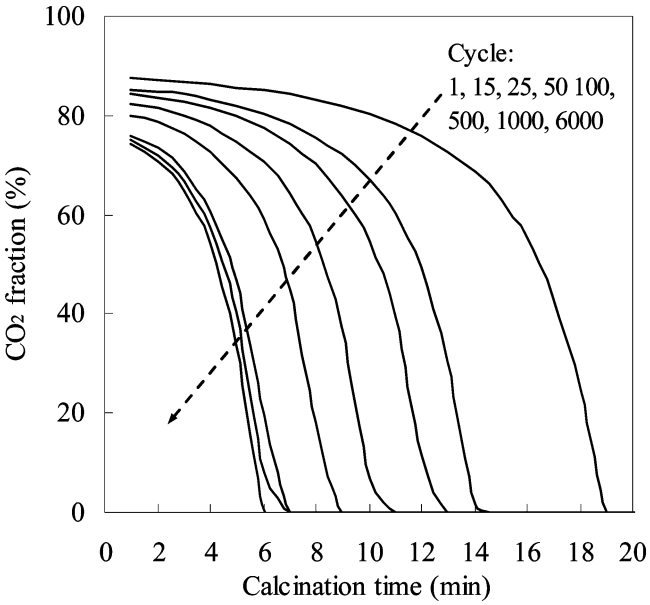

Figure 16. Evolution of CO_2 fraction with calcination time during sorbent regeneration period for different cycles (sorbent is CaO/$Ca_{12}Al_{14}O_{33}$, steam flow rate = 50 mL/min, calcination temperature = 1183 K).

regeneration process with 50 mL of steam per minute as the purge gas. With the increase in calcination temperature, the CO_2 fraction increases, while the time for $CaCO_3$ complete decomposition decreases, as shown in Figure 15. This is because both k_{calci} and P_{e,CO_2} increase with the increase in calcination temperature, resulting in the accelerated CO_2 decomposition rate.

The $CaCO_3$ decomposition process has been affected by the CO_2 partial pressure and calcination temperature; these parameters should be determined on the basis of the required time for the complete sorbent regeneration step in the practical process.

The cyclic reaction simulation results of the CO_2 fraction during the calcination step with CaO/$Ca_{12}Al_{14}O_{33}$ as the sorbent are shown in Figure 16. With the increase in cyclic number, the mass of $CaCO_3$ formed during the reforming step declines due to the loss of the sorbent activity; therefore, the CO_2 fraction in a gas atmosphere during the calcination step decreases with an increase in the cycle number. At the same time, the time for $CaCO_3$ decomposition also decreases with an increase in the cycle number, as shown in Figure 16.

5. Conclusions

In this work, the reactor model considering multiple cyclic carbonation/calcination reactions to analyze the SERP reactor system was developed and validated with experimental data. Using this model, the variation characteristics of the product gases evolution profile with reaction time, the effect of repeated carbonation/calcination number on SERP, and the effects of operational conditions and sorbent activity decay on the calcination process were investigated.

The simulated results indicate that, to achieve the advantages of SERP, the decrease in prebreakthrough time with the increase in the carbonation/calcination cycle of the sorbent must be considered. The prebreakthrough time declines continuously with the increase in cyclic number for three types of Ca-based sorbents, due to the loss of the sorbent activity. With a further increasing of the cycle, the prebreakthrough time will remain nearly constant, due to the sorbent already reaching the final residual capture capacity. The final prebreakthrough time is different for different sorbents, and this is very important in designing and operating the SERP system. Among the three sorbents, CaO/$Ca_{12}Al_{14}O_{33}$ obtains the highest final prebreakthrough time. Limestone and dolomite suffer from a rapid decline of sorption capacity, resulting in a low final prebreakthrough time. The effect of Ca-based sorbent activity decay on SERP must be considered in the reactor design and operation periods. It is obvious that a synthesized sorbent with high performance and a low cost would be highly beneficial for the sorption-enhanced hydrogen production process.

The $CaCO_3$ decomposition process in a fixed bed reactor has been affected by the CO_2 partial pressure and calcination temperature; these parameters should be determined on the basis of the required time for a complete sorbent regeneration step in the practical process.

Acknowledgment. This work was supported by the National High Technology Development Program of China (No. 2003AA501330) and National Basic Research Program of China (No. 2006CB705807).

Nomenclature

C_i = concentration of component i, kmol/m^3
$C_{i,f}$ = concentration of component i in the feed, kmol/m^3
$C_{i,init}$ = initial concentration of component i, kmol/m^3
C_{pg} = heat capacity of gas, kJ/kmol K
C_{ps} = heat capacity of solid, kJ/kmol K
d_p = particle diameter, m
k = the coefficient of sorbent activity loss
k_{calci} = apparent rate constant of $CaCO_3$ calcination, s^{-1}
k_c = apparent rate constant of CaO carbonation, s^{-1}
M_{CaO} = molecular weight of CaO, kg/kmol
M_{CaCO_3} = molecular weight of $CaCO_3$, kg/kmol
N = the cyclic number of carbonation/calcination for Ca-based sorbent
P_{0,CO_2} = partial pressure of CO_2, Pa
P_{e,CO_2} = partial equilibrium pressure of CO_2, Pa
P_i = partial pressure of gas-phase component i, Pa
r_0 = sorbent particle radius, m
R_0 = inner radius of reactor, m
R_{calci} = rate of CO_2 release by $CaCO_3$ calcination, kmol/kg-$CaCO_3$ s
$R_{cbn,N}$ = rate of CO_2 removal by CaO carbonation for N cycle, kmol/kg-CaO s
R_j = rate of reaction j(j = I, II, III), kmol/kg-cat s
t = time, s
T = temperature, K
T_f = feed gas temperature, K
T_{init} = initial temperature of reactor bed, K
T_W = reactor wall temperature, K
u = superficial velocity of gas, m/s
W_{CaCO_3} = weight of $CaCO_3$ after reforming reaction, kg
W_{cat} = weight of catalyst, kg
W_{sor} = weight of sorbent, kg
X_{active} = the fraction of CaO in Ca-based sorbent
X_{calci} = the decomposition conversion of $CaCO_3$
X_N = fractional carbonation conversion of CaO in N cycles
$X_{u,N}$ = ultimate fractional carbonation conversion of CaO in N cycles
z = axial coordinate in bed, m

Greek Letters

$\Delta H_{carbo,CO_2}$ = reaction heat of CaO carbonation, kJ/kmol
$\Delta H_{calci,CO_2}$ = reaction heat of $CaCO_3$ calcination, kJ/kmol
$\Delta H_{R,j}$ = reaction heat of reforming and shift reactions (j = I, II, III), kJ/kmol
ϵ_b = bed void fraction, dimensionless
η_j = catalyst effectiveness factor of reforming and shift reactions (j = I, II, III), dimensionless
$\eta_{sorbent}$ = sorbent effectiveness factor, dimensionless
$\rho_{b,sor}$ = apparent density of sorbent, kg/m^3
$\rho_{b,cat}$ = apparent density of catalyst, kg/m^3
$\rho_{b,CaO}$ = apparent density of CaO, kg/m^3
$\rho_{b,CaCO_3,N}$ = apparent density of $CaCO_3$ in N cycle, kg/m^3
ρ_g = density of gas, kg/m^3
ρ_s = average apparent density of sorbent and catalyst in reactor, kg/m^3

EF070112C